Terahertz emission from Mg-doped a-plane InN

H. Ahn*[a], Y.-J. Yeh[a], and S. Gwo[b]
[a]Department of Photonics and Institute of Electro-optical Engineering, National Chiao Tung University, Hsinchu 30010, Taiwan, Republic of China; [b]Department of Physics, National Tsing Hua University, Hsinchu 30013, Taiwan, Republic of China

ABSTRACT

We report terahertz (THz) emission from magnesium doped *a*-plane indium nitride (*a*-InN:Mg) films with different background carrier density, relative to the Mg-doped InN films grown along the *c*-axis (*c*-InN:Mg). Due to its high electron affinity, as-grown InN film is typically *n*-type and it has extremely high background carrier density, which causes much weaker THz emission than that from other semiconductors, such as InAs. The background carrier density of Mg-doped InN can be widely changed by adjusting the Mg doping level. For *c*-InN:Mg, THz emission is dramatically enhanced (×500 than that of undoped *c*-InN) as the background carrier density decreases to a critical value of $\sim 1\times10^{18}$ cm^{-3}, which is due to the reduced screening of the photo-Dember field at the lower carrier density. For *a*-InN, however, intense THz emission (×400 than that of undoped *c*-InN) is observed for both undoped and Mg-doped *a*-InN and the enhancement is weakly dependent on the background carrier density. The primary THz radiation mechanism of the *a*-plane InN film is found to be due to the acceleration of photoexcited carriers under the polarization-induced in-plane electric field perpendicular to the *a*-axis, which effectively enhances the geometrical coupling of the radiation out of semiconductor. The weak dependence of THz radiation on the background carrier density for *a*-InN shows that in-plane surface field induced-terahertz emission is not affected by the background carrier density. Small, but apparent azimuthal angle dependence of terahertz emission is also observed for *a*-InN, indicating the additional contribution of nonlinear optical processes on terahertz emission.

Keywords: nonpolar indium nitride, terahertz emission, in-plane electric field

1. INTRODUCTION

It is known that photoexcited carriers generated close to the surface of semiconductors can be accelerated by an appropriate electric field and the resultant transient electric dipole can lead to generation of THz pulses. The proper electric field can be provided either externally by separate electrodes in photoconductive antennas or internally by the photo-Dember field or by the electron accumulation field. THz emission due to the photo-Dember effect and surface field acceleration depends closely on carrier concentration. For the narrow bandgap semiconductors with high background carrier density, THz emission can be seriously limited by the strong screening of the photo-Dember field.[1,2] Since the discovery of its narrow intrinsic bandgap, indium nitride (InN) has received much attention in THz range applications due to its high electron mobility and low interband absorption. However, because of its large electron affinity, as-grown InN film is typically *n*-type and has an extremely high background carrier density ($n\sim10^{17}$–10^{18} cm^{-3}). Therefore, THz emission from as-grown *c*-plane InN (*c*-InN) is typically much weaker than that from other semiconductors, such as InAs.[3-6] The reduction of THz intensity with the increase of the carrier density has been observed for as-grown and Si-doped InN.[7] Doping InN with proper acceptors, such as Mg, is expected to reduce the carrier density and enhance the radiation intensity. Recently, we have demonstrated the drastic enhancement of the THz radiation from magnesium (Mg) doped *c*-InN, in which Mg works as an acceptor dopant to reduce the background carrier density.[8] Meanwhile, the surge current-induced THz radiation from *c*-InN is limited not only by the high background carrier density, but also by the low light-extraction efficiency due to large total internal reflection occurring within a material of high refractive index.[9] Nanostructures with higher surface-to-volume ratio can increase the THz emission efficiency by increasing the effective emission surface.[3] In addition, at least two orders of magnitude enhancement of THz generation has been observed from nonpolar InN grown along the *a*-axis (*a*-InN) and THz generation from *a*-InN is known to be dominated by the polarization-induced in-plane electric field combined with an optical nonlinear effect.[10] THz signals by in-plane dipole oscillation can be favorably coupled to a narrow emission cone and can surpass the surge-current-induced THz radiation.

*hyahn@mail.nctu.edu.tw; phone 886 3 5712121-56369; fax 886 3 5716631

Quantum Sensing and Nanophotonic Devices VIII, edited by Manijeh Razeghi, Rengarajan Sudharsanan, Gail J. Brown, Proc. of SPIE Vol. 7945, 79450Z · © 2011 SPIE · CCC code: 0277-786X/11/$18 · doi: 10.1117/12.874400

Downloaded From: http://proceedings.spiedigitallibrary.org/ on 04/24/2014 Terms of Use: http://spiedl.org/terms

Similarly high intensity enhancement has been achieved by applying an external magnetic field parallel to the semiconductor surface,[11-13] in which the dipole radiation field can be rotated to increase the extraction efficiency. Meanwhile, for nonpolar (*a*- and *m*-plane) InN photoexcited at a relatively lower excitation fluence (~$\mu J/cm^2$), Metcalfe *et al*. proposed another emission mechanism which is attributed the drift of carriers in an intrinsic in-plane electric field.[14] In this mechanism, the intrinsic in-plane electric field is induced by the high-density stacking fault of nonpolar InN along *c*-axis and the rotation of the sample by 180˚ flips the polarity of THz field due to the acceleration of carriers in the opposite direction. The THz intensity of angular independent component due to the photo-Dember effect from nonpolar InN was found to be much smaller than that of angle dependent one.

Typically, due to the very thin electron accumulation layer at the surface (<10 nm), the contribution of the electron acceleration field to the THz generation from *c*-InN is negligibly small and the photo-Dember field dominates THz emission. However, THz emission from Mg-doped *c*-InN is alternatively determined by the photo-Dember field and the surface electron acceleration field depending on the background carrier density.[8] Meanwhile, our previous result on THz generation from *a*-InN shows an asymmetric four-fold rotation symmetry, which is in contrast to the simple sinusoidal dependence of THz field from nonpolar InN with a high stacking fault density. However, the background carrier density dependence of THz field from Mg-doped *a*-InN has not been investigated. In this paper we investigated the THz emission from the *a*-InN films doped with Mg (*a*-InN:Mg). The *a*-InN:Mg films with various background carrier densities were prepared by growing the samples at different Mg cell temperatures and the photocarrier density dependence of THz generation is investigated by measuring THz emission from the samples photoexcited at different pump fluences. In sharp contrast to *c*-InN:Mg case, THz emissions from the *a*-InN:Mg films with different background carrier densities are comparable to that from undoped *a*-InN and more importantly, do not sharply decrease with the increase of carrier density, indicating the negligible contribution of the photo-Dember effect to the THz generation from *a*-InN:Mg.

2. EXPERIMENTAL METHOD

2.1 Experimental set-up

Time-domain THz emission measurements were performed using a Ti:sapphire regenerative amplifier laser system, which delivers ~50 fs optical pulses at a center wavelength of 800 nm with a repetition rate of 1 kHz. For this experiment, the pump laser beam is collimated on the samples with a spot size of ~ 2 mm at the incident angle of 70˚. The transient photoexcitation initiates coherent plasma oscillations of the photoexcited carriers in the samples, which leads to the emission of few-cycle THz pulses. The terahertz pulses were detected by free-space electro-optic sampling in a 2-mm-thick ZnTe crystal as a function of delay time with respect to the optical pump pulse. A balanced detector detects the differential photocurrent as a function of time delay between the THz pulses and optical probe beam. All the measurements were done under dry nitrogen. The experimental details of THz emission measurement system can be found elsewhere.[15]

Near-infrared photoluminescence (PL) from the Mg-doped *a*- and *c*-plane InN films at room temperature was measured by a 1/4-m spectrometer equipped with a 600 g/mm grating and a liquid-nitrogen-cooled charge-coupled-device (CCD) detector. The samples were photoexcited by the normally incident femtosecond laser pulses which delivers ~150 fs laser pulses at the repetition rate of 82 MHz with the center wavelength of 800 nm. All of the PL spectra have been corrected by the system response curve. We also have investigated the azimuthal angle dependence of THz emission from *c*- and *a*-plane InN films. At high pump fluence, optical nonlinear effect-induced THz emission from the semiconductor surfaces shows the characteristic azimuthal angle dependence.

2.2 Sample preparation

For this work, several *a*-InN and *a*-InN:Mg films (with a nominal thickness of ~1.2 μm) were grown on *r*-plane $\{1\bar{1}02\}$ sapphire substrates, whereas –*c*-plane $(000\bar{1})$ undoped and Mg-doped InN films with a thickness of ~ 1.2 μm were grown on Si(111) substrates by plasma-assisted molecular beam epitaxy. Mg doping was performed with a high-purity Mg (6N) Knudsen cell and the Mg doping level was controlled by regulating the cell temperature between 180 and 290 ˚C. The electron density and mobility of undoped *a*-InN film determined by room-temperature electron Hall effect measurement are ~7×10^{18} cm^{-3} and 300 cm^2/Vs, respectively. The electron density and mobility of *c*-InN:Mg and *a*-InN:Mg are subject to the Mg doping level and their dependence on the Mg cell temperature is illustrated in Fig. 1. In

Downloaded From: http://proceedings.spiedigitallibrary.org/ on 04/24/2014 Terms of Use: http://spiedl.org/terms

this figure, the carrier density and electron mobility at zero Mg cell temperature correspond to those of undoped *c*- and *a*-InN films. Here, the carrier density shows a peculiar V-shape dependence on the Mg doping level in such a way that the carrier density first decreases as the Mg cell temperature increases and then increases at higher Mg cell temperatures due to strong longitudinal optical phonon-plasmon coupling.[16] For *a*-InN:Mg doped at Mg cell temperatures >250 ˚C, the carrier density can be even higher than that of undoped *a*-InN.

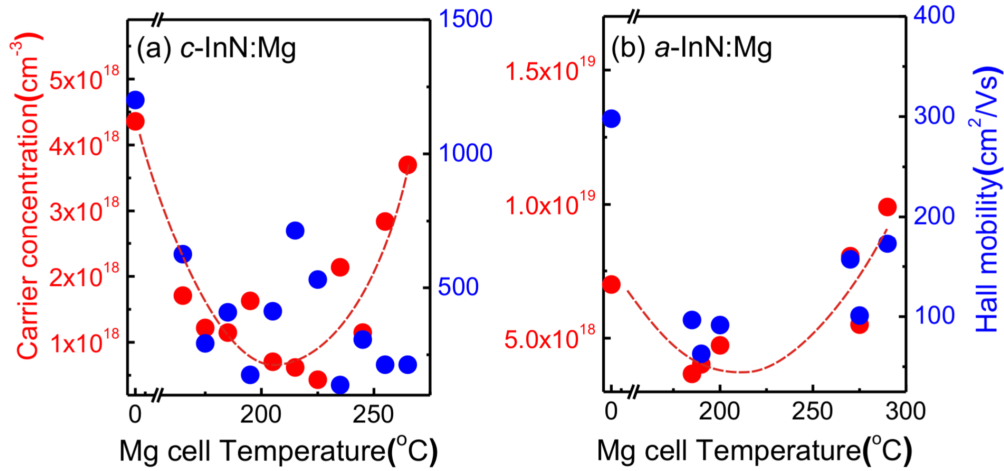

Fig. 1. Background carrier concentration and electron Hall mobility of (a) *c*- and (b) *a*-InN:Mg as a function of Mg cell temperature. V-shape dependence of carrier concentration can be observed for both samples.

Meanwhile, InN films grown at a high Mg cell temperature is often accompanied by inferior crystalline quality. The room-temperature PL intensity of InN in Fig. 2 exhibits that InN films grown at the Mg cell temperature >180 ˚C do not have observable PL, while the strong PL was found in undoped InN. This drastic reduction of PL may indicate the degradation of crystalline quality by the high temperature Mg doping. A separate measurement of THz time-domain spectroscopy of Mg-doped InN also shows that Mg doping causes the serious structural disordering. (not shown)

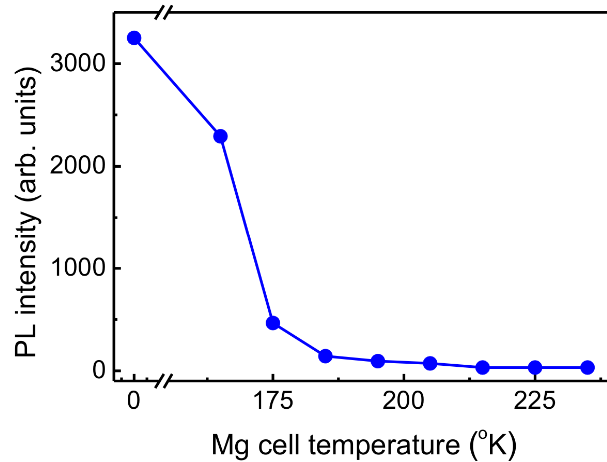

Fig. 2. The peak intensity of room-temperature photoluminescence of the Mg-doped InN films as a function of Mg cell temperature. At the cell temperature >180 ˚C, PL intensity could not be measured by our CCD detector.

Downloaded From: http://proceedings.spiedigitallibrary.org/ on 04/24/2014 Terms of Use: http://spiedl.org/terms

3. TERAHERTZ EMISSION MEASUREMENT

Figure 3 shows the peak amplitude of *p*-polarized THz field waveform from the *a*- and *c*-InN:Mg films as a function of background carrier density. For *c*-InN:Mg, THz emission with positive polarity is sharply enhanced as n decreases from that of undoped *c*-InN and with the carrier density below $n_c \sim 1\times10^{18}$ cm^{-3}, the THz amplitude begins to decrease again and its polarity changes to a negative sign. The terahertz polarity of the sample is confirmed by comparing it with those of *n*- and *p*-type GaAs wafers, which shows the opposite signs of polarity depending on the doping type.[8] The intensity (square of amplitude) of THz radiation from *c*-InN:Mg with $\sim n_c$ is at least 500 times stronger than that from undoped *c*-InN (open square symbol) and it is nearly the same as that from an *n*-type InAs (100) film with $n \sim 10^{17}$ cm^{-3} (triangle symbol). THz generation associated with the surge current depends on the densities of both background and photoexcited carriers through the relation,[17]

$$J = J_E + J_D = eE(n_t\mu_n + p_t\mu_p) + e(D_n\nabla n_t - D_p\nabla p_t)\,, \tag{1}$$

where n_t (p_t) includes both background carriers and photoexcited carriers, and μ_n (μ_p) and D_n (D_p) correspond to the mobility and the diffusion coefficient of electrons (holes), respectively. Since InN has the downward surface band-bending, THz field due to the surface electric field always shows the negative polarity, while THz field due to the photo-Dember effect has the positive polarity. The fast decay of THz signals from *c*-InN:Mg with the increase of the background carrier density and the flip of the polarity indicates the interplay of the diffusion and drift currents, which direct the outward and inward directions of the InN film, respectively.[8]

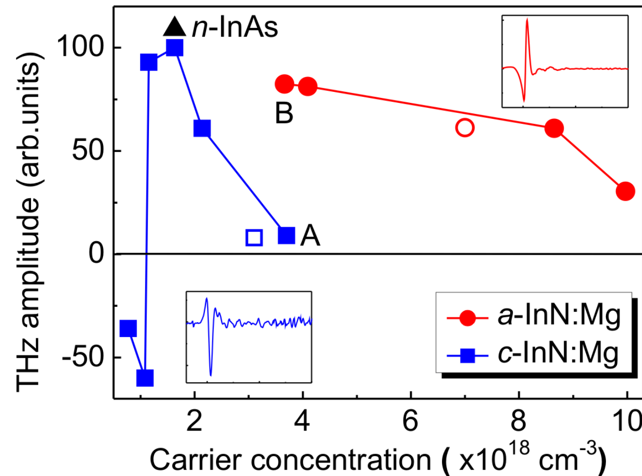

Fig. 3. The peak amplitudes of THz field from *a*- and *c*-InN:Mg compared with those of undoped *a*- and *c*-InN. Negative values of THz amplitude correspond to negative THz polarity which is shown in a lower inset.

Meanwhile, the carrier density dependence of the THz radiation of *a*-InN:Mg shown in Fig. 3 is different from that of *c*-InN:Mg in several ways. First, the amplitude of the THz field from *a*-InN:Mg is as high as that from an undoped *a*-InN (shown by an open circle in Fig. 3) which is about ten times (a hundred times in intensity) stronger than that from the undoped *c*-InN and it does not sharply drop as the carrier density increases as high as $\sim 1\times10^{19}$ cm^{-3}. Second, the polarity of the THz signals from *a*-InN:Mg is all positive and it does not change the sign with the variation of the carrier density. Positive polarity of THz field from *a*-InN:Mg excludes the contribution of surface electric field due to the downward surface band-bending.

In order to separately identify the contribution of the photo-Dember effect to the THz generation from *a*-InN:Mg, we prepared a *c*-InN:Mg (sample A) film and an *a*-InN:Mg (sample B) film with a similar background carrier density $\sim 3.5\times10^{18}$ cm^{-3}. Since each sample in Fig. 2 is excited at the same pump fluence, samples A and B have not only the same background carrier density, but also the same photoexcited carrier density. If the THz emission from *a*-InN:Mg is solely due to the photo-Dember effect, according to eq.(1), the THz generation from samples A and B with the same

Downloaded From: http://proceedings.spiedigitallibrary.org/ on 04/24/2014 Terms of Use: http://spiedl.org/terms

background and photoexcited carrier densities should be similar. Contrary to the expectation, Fig. 3 shows that the THz signal from sample B is at least ten times stronger than that from sample A, indicating that the THz generation from *a*-InN:Mg is not due to the photo-Dember field, but due to another emission mechanism which does not depend on the carrier density. We attribute the major THz generation mechanism of *a*-InN:Mg to carrier transport in an in-plane electric field, the same as that of an undoped *a*-InN. Since the proposed in-plane electric field is due to the anisotropic charge distribution between In and N atoms in the basal plane, the magnitude of THz field from *a*-InN:Mg would depend on the density of In-N pairs instead of the background charge carrier density. Slight increase of THz amplitude with the decrease of the carrier density may be due to the reduction of screening, and the decrease of THz amplitude at the carrier density may be due to the deterioration of crystal quality during the doping of Mg at high Mg cell temperature.

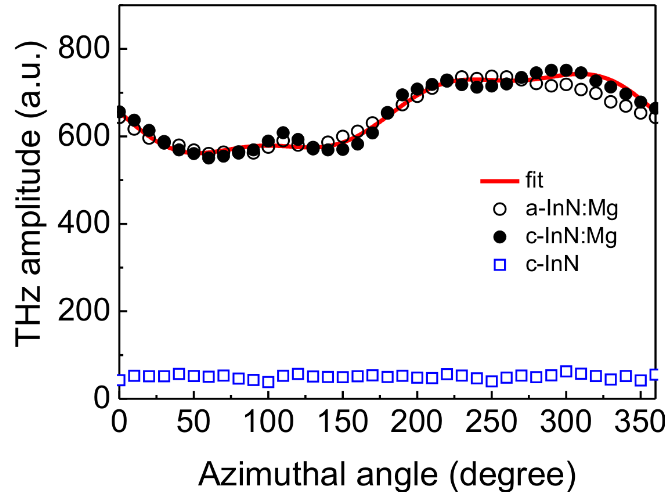

Fig. 4. The peak amplitudes of THz field from *a*- and *c*-InN:Mg as a function of the azimuthal angle rotation of the samples. The red solid line is the result of fitting based on the bulk and surface second order susceptibility tensor elements of *a*-InN.[10]

Optical rectification is typically dominant in terahertz emission from wide-bandgap materials, but it becomes significant for narrow bandgap semiconductors photoexcited at high pump fluence. For optical rectification, the second-order optical susceptibilities $\chi^{(2)}$ of semiconductors are exploited for the production of a time-dependent polarization and generate terahertz radiation. The intensity of optical rectification-induced terahertz radiation varies as the samples rotate about the surface normal according to the azimuthal angle dependence of $\chi^{(2)}$, distinguishing it from the current surge mechanisms. Figure 4 shows the *p*-polarized THz amplitude from *a*-InN:Mg excited by *p*-polarized pump as a function of azimuthal rotation angle θ of the sample. THz signals from *a*-InN:Mg show the similar four-fold angular dependence to that from undoped *a*-InN,[10] whereas that of *c*-InN:Mg is angular independent. The fitting curve in Fig. 4 is obtained by including the contribution of the surface as well as bulk second-order optical susceptibility elements. The contribution of optical rectification becomes significant as the pump fluence is increased and it is illustrated in Fig. 5. Here, in order to isolate the angular dependent component from the angular-independent one, we plotted the THz amplitudes at two azimuthal angles θ_1 and θ_2, where the angular modulation of THz field is zero and maximum, respectively. For both cases, THz signals increases linearly with the increase of the pump fluence, indicating that our pump fluence is well below the regime of photocarrier saturation. Figure 5 also shows that the THz radiation measured at θ_2 increases faster than that at θ_1 as the pump fluence is increased. Linear increase of THz radiation measured at θ_1 is due to the increase of photoexcited carriers, while a larger linear slope of terahertz radiation at θ_2 indicates that a nonlinear optical effect contribution becomes more pronounced as the pump fluence is increased. The angular dependence of *a*-In:Mg in Fig. 5 is different from the simple $\sin\theta$ dependence of THz field reported by Metcalfe *et al.*[14] for nonpolar InN films excited at a low fluence (1−50 μJ/cm^2). The nonpolar InN films studied by Metcalfe *et al.* has a high stacking-fault density and the $\sin\theta$ dependence of THz response is proposed to be due to a stacking fault-terminated internal polarization at wurzite domain boundaries parallel to *c*-axis. The same authors have also reported that nonpolar GaN films with a high stacking-

Downloaded From: http://proceedings.spiedigitallibrary.org/ on 04/24/2014 Terms of Use: http://spiedl.org/terms

fault density show the similar sinθ dependence, while nonpolar GaN films with a low stacking-fault density do not show the azimuthal angle dependence.[18] Meanwhile, the angular dependent component of the *a*-InN:Mg film in Fig. 5 becomes barely detectable when the pump fluence is reduced to <100 μJ/cm^2, indicating that the THz emission from our *a*-InN:Mg films is not affected by the stacking-fault density.

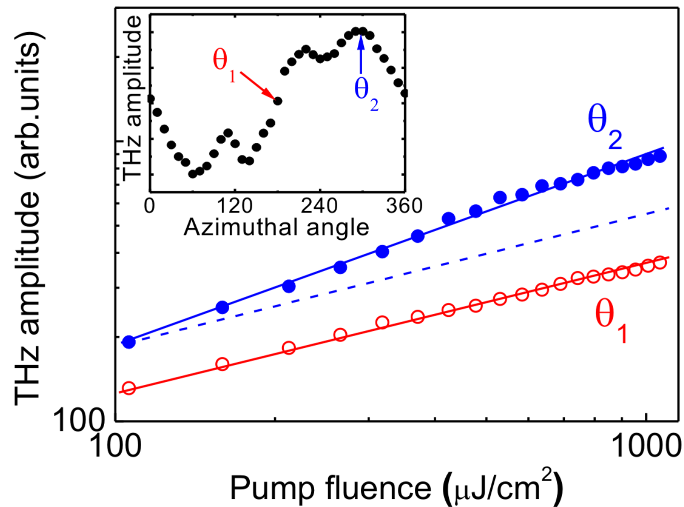

Fig. 5. The amplitudes of the THz field vs. pump fluence measured at the azimuthal angles, θ_1 and θ_2, where angular modulation of THz field is zero and maximum, respectively.

4. SUMMARY

It has been found that the Mg-doped *a*-plane InN film radiates about 100 times more intense THz pulses compared to that of the undoped *c*-plane InN film and the amplitude of THz radiation from Mg-doped *a*-plane InN film is insensitive to the variation of the background carrier density determined by the doping level of Mg. The major THz emission mechanism is originated from the polarization-induced in-plane electric field which accelerates the carriers along the nonpolar surface. The contribution of the photo-Dember effect which dominates THz emission from Mg-doped *c*-InN is insignificant for Mg-doped *a*-InN. The distinctive azimuthal angle dependence of the terahertz field from the Mg-doped *a*-plane InN film is similar to that from undoped *a*-plane InN which is attributed to optical rectification.

ACKNOWLEDGEMENTS

This work was supported by the National Science Council (NSC 98-2112-M-009-009-MY3) and the National Nanoscience and Nanotechnology Project (NSC 98-2120-M-007-009) in Taiwan.

REFERENCES

[1] K. Liu, J. Xu, T. Yuan, and X.-C. Zhang, “Terahertz radiation from InAs induced by carrier diffusion and drift,” Phys. Rev. B **73**, 155330 (2006).

[2] R. Ascazubi, C. Shneider, I. Wilke, R. Pino, and P. S. Dutta, “Enhanced terahertz emission from impurity compensated GaSb,” Phys. Rev. B, **72**, 045328 (2005).

[3] H. Ahn, Y.-P. Ku, Y.-C. Wang, C.-H. Chuang, S. Gwo, and C.-L. Pan, “Terahertz Emission from Vertically Aligned InN Nanorod Array,” Appl. Phys. Lett. **91**, 132108 (2007).

[4] I. Wilke, R. Ascazubi, H. Lu, and W. J. Schaff, “Terahertz emission from silicon and magnesium doped indium nitride,” Appl. Phys. Lett. **93**, 221113 (2008).

Downloaded From: http://proceedings.spiedigitallibrary.org/ on 04/24/2014 Terms of Use: http://spiedl.org/terms

[5] G. D. Chern, E. D. Readinger, H. Shen, M. Wraback, C. S. Gallinat, G. Koblmüller, and J. S. Speck, "Excitation wavelength dependence of terahertz emission from InN and InAs," Appl. Phys. Lett. **89**, 141115 (2006).
[6] R. Acsazubi, I. Wilke, K. Denniston, H. L. Lu, and W. J. Schaff, "Terahertz emission by InN," Appl. Phys. Lett. **84**, 4810 (2004).
[7] R. Ascazubi, I. Wilke, S. Cho, H. Lu, and W. J. Schaff, "Ultrafast recombination in Si-doped InN," Appl. Phys. Lett. **88**, 112111 (2006).
[8] H. Ahn, Y.-J. Yeh, Y.-L. Hong, and S. Gwo, "Terahertz emission mechanism of magnesium doped indium nitride," Appl. Phys. Lett. **95**, 232104 (2009).
[9] M. B. Johnston, D. M. Whittaker, A. Corchia, A. G. Davies, and E. H. Linfield, "Simulation of terahertz generation at semiconductor surfaces," Phys. Rev. B **65**, 165301 (2002).
[10] H. Ahn, Y.-P. Ku, C.-H. Chuang, C.-L. Pan, H.-W. Lin, Y.-L. Hong, and S. Gwo, "Intense terahertz emission from *a*-plane InN surface," Appl. Phys. Lett. **92**, 102103 (2008).
[11] X. C. Zhang, Y. Liu, T. D. Hewitt, T. Sangsiri, L. E. Kingsley, and M. Weiner, "Magnetic switching of THz beams," Appl. Phys. Lett. **62**, 2003 (1993)
[12] P. Gu, M. Tani, S. Kono, K. Sakai, and X. C. Zhang, "Study of THz radiation from InAs and InSb," J. Appl. Phys. **91**, 5533 (2002).
[13] S. C. Howells, S. D. Herrera, and L. A. Schlie, "Infrared wavelength and temperature dependence of optically induced terahertz radiation from InSb," Appl. Phys. Lett. **65**, 2946 (1994).
[14] G. D. Metcalfe, H. Shen, M. Wraback, G. Koblmüller, C. Gallinat, F. Wu, and J. S. Speck, "Terahertz Radiation from Nonpolar InN Due to Drift in an Intrinsic In-Plane Electric Field," Appl. Phys. Exp. **3**, 092201 (2010)
[15] H. Ahn, C.-L. Pan, and S. Gwo, "Terahertz emission and spectroscopy on InN epilayer and nanostructure," Proc. of SPIE, **7216**, 72160T (2009).
[16] M. Fujiwara, Y. Ishihiro, X. Wang, S.-B. Che, and A. Yoshikawa, "Infrared analysis of hole properties of Mg-doped *p*-type InN films," Appl. Phys. Lett. **93**, 231903 (2008).
[17] J. N. Heyman, N. Coates, and A. Reinhardt, "Diffusion and drift in terahertz emission at GaAs surfaces," Appl. Phys. Lett. **83**, 5476 (2003).
[18] G. D. Metcalfe, H. Shen, M. Wraback, A. Hirai, F. Wu, and J. S. Speck, "Enhanced terahertz radiation from high stacking fault density nonpolar GaN," Appl. Phys. Lett. **92**, 241106 (2008).

Downloaded From: http://proceedings.spiedigitallibrary.org/ on 04/24/2014 Terms of Use: http://spiedl.org/terms